Electronic Supplementary Information (ESI) for

Operando chemical strain analysis of CNT/VOOH during zinc insertion for Zn-ion batteries

Xiuling Shi, [a] Yuchuan Sun,[a] Yibo Weng,[a] Xiaoying Long, [a] Tongxing Lei,[a] Jianli Zhou,[b] Deping Li,[a] Jin Zhang,[b] Yan Huang, *[a] Lijie Ci,[a] Kaikai Li,*[a] Tong-Yi Zhang*[c]

[a.] School of Materials Science and Engineering, Harbin Institute of Technology, Shenzhen, China. Email: likaikai@hit.edu.cn, yanhuanglib@hit.edu.cn

[b.] School of Science, Harbin Institute of Technology, Shenzhen, 518055, China

[c.] Guangzhou Municipal Key Laboratory of Materials Informatics, Advanced Materials Thrust and Sustainable Energy and Environment Thrust, The Hong Kong University of Science and Technology (Guangzhou), Nansha, Guangzhou, 511400, Guangdong, China. E-mail: zhangty@shu.edu.cn

Experimental Section

Materials Preparation: Carbon nanotubes (CNTs) were purchased from Shenzhen Nanotech Port Co. Ltd, and were refluxed in nitric acid (65 wt%) at 140 °C for 6 h. [1] 10 mg acid-CNTs were dispersed in 30 ml of water with sonication for 1 h, followed by addition of 2 mmol NH_4VO_3 and 2 ml $NH_3 \cdot H_2O$. Then, 15 mmol C_2H_5NS was added into the above mixed solution, and stirred for 1 h. The obtained solution was transferred into a Teflon-lined stainless steel autoclave for hydrothermal treatment at 180 °C for 24 h. The final products were washed three times with water and ethanol and dried at 60 °C overnight. For comparison, bare VOOH was synthesized with the same synthesis procedure but without the addition of CNTs.

Electrochemical Measurements: Electrochemical performance were tested using a CR2032 type coin cell assembled in air. The working electrode was prepared by mixing active material (70 wt%), acetylene black (20 wt%) and polytetrafluoroethylene (PVDF, 10 wt%) in N-Methylpyrrolidone (NMP). The obtained slurry was cast onto carbon cloth and dried in a vacuum oven at 110 °C for 12 h. The mass loading of the active material in each electrode was 1.5~2 mg cm^{-2}. Zinc foil and glass fiber membrane were used as anode and separator, respectively, and 3 M zinc triflate solution was used as electrolyte. The galvanostatic cycling test was performed on the Neware battery test system (CT-4008T, Shenzhen, China). Cyclic voltammetry (CV) and electrochemical impedance spectroscopy (EIS) measurements were measured by EC-lab electrochemical workstation. The specific capacity was calculated based on the total mass of the CNT/VOOH composite material.

Materials Characterizations: The phase composition and transformations of the samples were characterized by X-ray diffractometer (XRD; PANalytical Aeris) with Cu Kα radiation at 0.15418 nm and a scan range of 5-80°. Microstructural and morphological characterizations were investigated by field emission scanning electron microscopy (SEM, ZEISS GeminiSEM 300) and transmission electron microscopy (FEI Tecnai G2 F30). An energy dispersive X-ray spectrometer equipped SEM was used for elemental analysis. Elemental quantification was performed by an inductively coupled plasma mass spectrometer Agilent 7700s (ICP-MS). XPS spectra were collected by X-ray photoelectron spectroscopy (K-Alpha, Thermo Fisher Scientific) and analyzed by calibrating C 1*s* to the 284.8 eV. Thermogravimetric analysis (TGA) was performed in the temperature range of 30-600 °C on a synchronous thermal analyzer (NETZSCH STA449F5). The Raman spectra were collected on a confocal Raman spectrometer (Renishaw inVia Qontor).

Operando Strain Measurements and Analyses: The design of the home-made operando chemical strain test system was described in our previous work. [2] The custom operando cell contained a quartz window that allowed optical access to the electrode surface. Zinc metal was used as the counter electrode. In order to shorten the diffusion path of the Zn ions in the electrolyte as much as possible, the flat Zn anode was placed on the bottom of the operando cell. Non-contact DIC technique was used to real-time measure the displacement/strain fields of the graphite electrode surface. Specifically, graphite particles were added in the cantilever electrode aiming to generate natural speckles, considering that the graphite does not participate in electrochemical reactions.

A series of optical images of the cantilever electrode surface were captured every 300 seconds using a CCD camera with a resolution of a 1624 × 1228 pixel, for an effective scale of ca. 2.15 μm pixel^{-1}. All the images were converted to black and white before correlation, and the first image, which was captured before the start of the discharge of the cell, was set as the reference image. The region of interest (ROI) was selected to be 2.5×2 mm^2. By correlating the position of pixel subsets in the reference and deformed images (normally based upon grey intensity levels), the displacements (δ_{xx} and δ_{yy}) and strains (ε_{xx} and ε_{yy}) over the ROI were computed using the Matlab-based DIC code developed by Elizabeth M. C. Jones. [3] For the displacement calculations, a grid of evenly spaced control points (in steps of 20 pixels) was defined on the ROI at the same coordinates in both the reference image and the deformed images. Then, the normalized cross-correlation coefficient, C, was computed by convolving the subset from the deformed image with the larger subset from the reference image. [3]

Prior to the strain calculations, the displacements were smoothed using a smoothing kernel of 11 × 11 control points around each control point, which were then weighted with a Gaussian distribution centered at the central control point and then averaged. [3] Next, the strains (ε_{xx} and ε_{yy}) can be calculated by

$$\varepsilon_{xx} = \frac{\partial \delta_{xx}}{\partial x} \quad and \quad \varepsilon_{yy} = \frac{\partial \delta_{yy}}{\partial y}. \qquad (1)$$

Electrochemical-mechanical coupling model: The total mole number of Zn, n_{Zn}, measured by the charging/discharging current and time, is called the nominal mole number. The chemical strain of electrode during Zn insertion is given by

$$e(n_{Zn}) = \frac{\int_0^{n_{Zn}} V_{Zn}^{in} dn_{Zn}}{V_0} \quad (2)$$

where $\bar{V}_{Zn}^{in}$ is the nominal partial molar volume of Zn in the electrode during Zn insertion. The measured linear strain ε is one third of the volumetric strain $\varepsilon = \frac{e}{3}$, i.e.,

$$\varepsilon(n_{Zn}) = \frac{\int_0^{n_{Zn}} \bar{V}_{Zn}^{in} dn_{Zn}}{3V_0} \quad (3)$$

The chemical strain includes reversible and irreversible strains. The chemical strain of electrode during Zn extraction is given by

$$\Delta\varepsilon_{out} = \left(\varepsilon_{max}\left(n_{Zn}^{max}\right) - \varepsilon_{out}\right) \quad (4)$$

where $\varepsilon_{max}\left(n_{Zn}^{max}\right)$ is the chemical strain induced by the maximum Zn mole number and

$$\varepsilon_{out} = \frac{\int_{n_{Zn}}^{n_{Zn}^{max}} V_{Zn}^{out} dn_{Zn}}{3V_0} \quad (5)$$

with $\bar{V}_{Zn}^{out}$ being the nominal partial molar volume of Zn in the electrode during Zn extraction. The Zn extraction ends at n_{Zn}^{min}. The experimentally measured value of n_{Zn}^{min} is actually the residual Zn mole number n_{Zn}^{res} and the experimentally measured value of chemical strain conjugated with n_{Zn}^{res} is called the residual strain $\varepsilon_{Zn}^{res}\left(n_{Zn}^{res}\right)$. The curve of strain versus capacity (Zn mole number) is approximately linear during Zn ion extraction. Extending the line of strain versus capacity (Zn mole number) during Zn ion extraction to $n_{Zn} = 0$, the intercept gives the plastic strain $\varepsilon_p(n_{Zn} = 0)$ generated in this charging/discharging cycle. Thus, the residual Zn mole number induces the purely residual strain ε_{Zn}^{pure}

$$\varepsilon_{Zn}^{pure} = \varepsilon_{Zn}^{res}\left(n_{Zn}^{res}\right) - \varepsilon_p(n_{Zn} = 0) \quad (6)$$

Assuming that all the residual Zn ions stay in the electrically active particles, we have

$$\varepsilon_{Zn}^{pure} = \frac{V_{Zn}^{a} n_{Zn}^{res}}{3V_0} = \frac{V_{Zn}^{a} C_{Zn}^{res} m_a}{3V_0 F} \quad (7)$$

where V_{Zn}^{a} is the partial molar volume of Zn in electrically active particles, F is the Faraday constant, C_{Zn}^{res} is the residual capacity, m_a is the mass of the electrically active particles in the studied electrode.

Figure S1. Schematic illustration of the synthesis of the CNT/VOOH composite.

Figure S2. Schematic illustration of the synthesis of the VOOH composite.

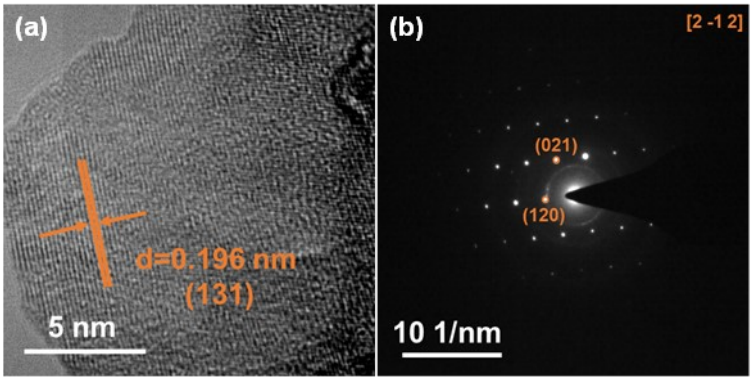

Figure S3. (a) HRTEM image and (b) SAED pattern of CNT/VOOH.

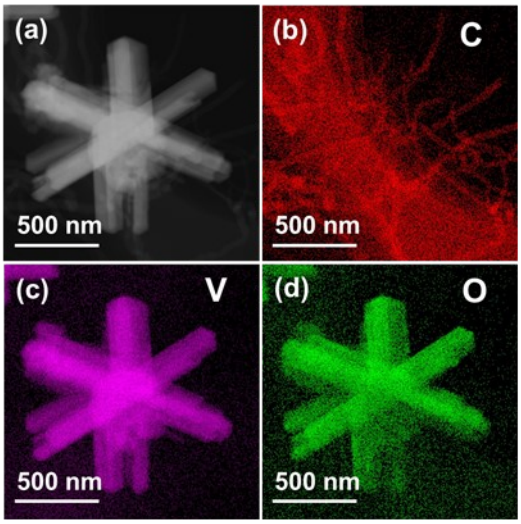

Figure S4. TEM image and corresponding EDS mapping images of CNT/VOOH.

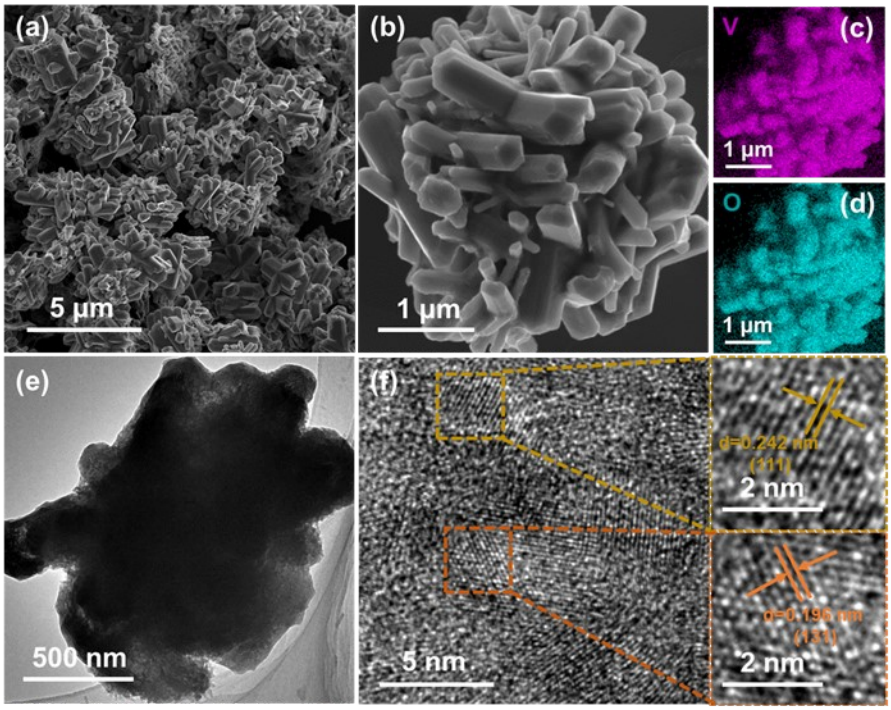

Figure S5. (a-b) SEM images and (c-d) elemental distribution of bare VOOH, (e) TEM image and (f) HRTEM image of bare VOOH.

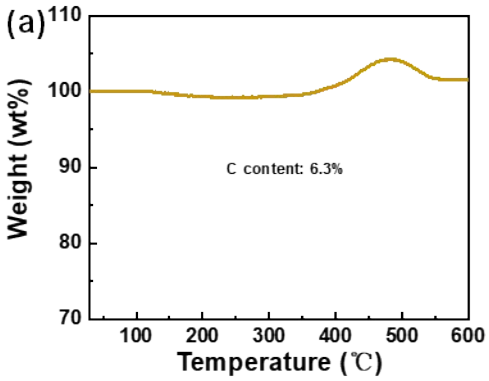

(b)

ICP-MS		
Sample	Element	Content
CNT/VOOH	V	52.99%
VOOH	V	58.85%

Figure S6. (a) TGA curves of CNT/VOOH. (b) V content of CNT/VOOH and VOOH measured by ICP-MS.

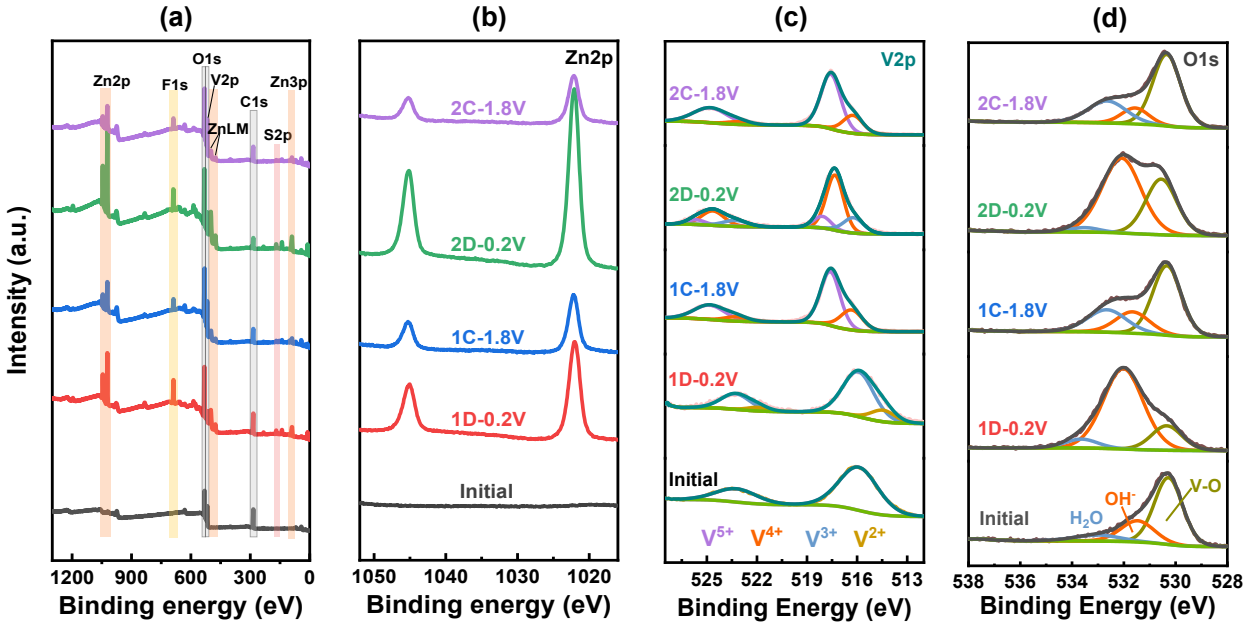

Figure S7. XPS profiles. (a) Survey spectra and high-resolution spectra of (b) Zn 2*p*, (c) V 2*p* and (d) O 1*s* of the CNT/VOOH composite cathode at different states.

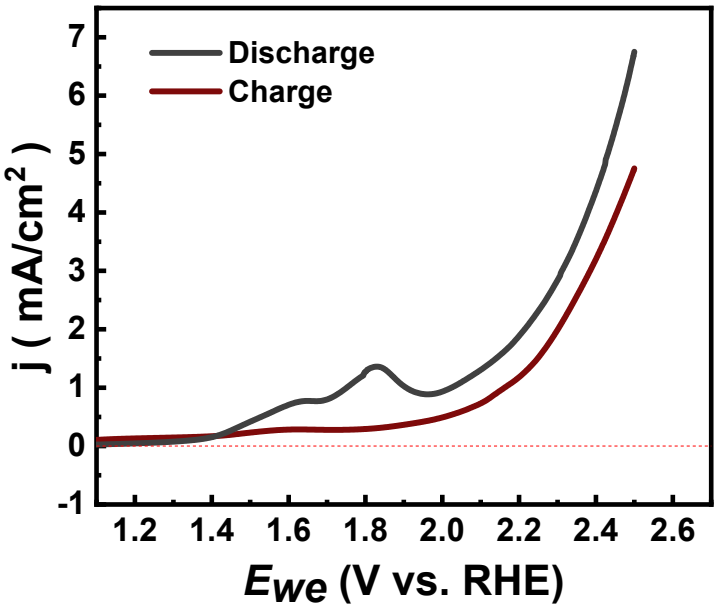

Figure S8. Linear sweep voltammetry (LSV) curves of the CNT/VOOH cathode after first discharge and first charge.

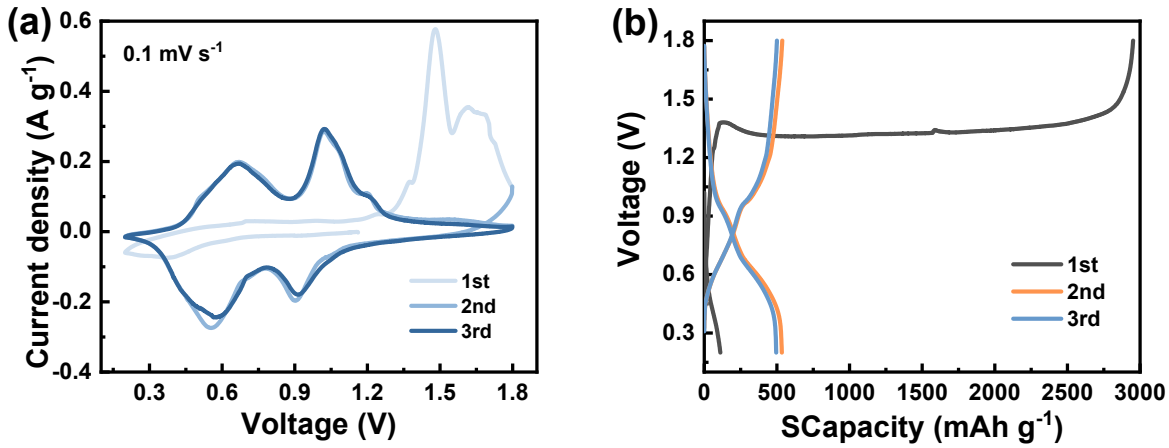

Figure S9. (a) CV curves of the VOOH electrode recorded at a scan rate of 0.1 mV s^{-1}. (b) Galvanostatic charge/discharge voltage profiles of the VOOH electrode at a current density of 0.1 A g^{-1}.

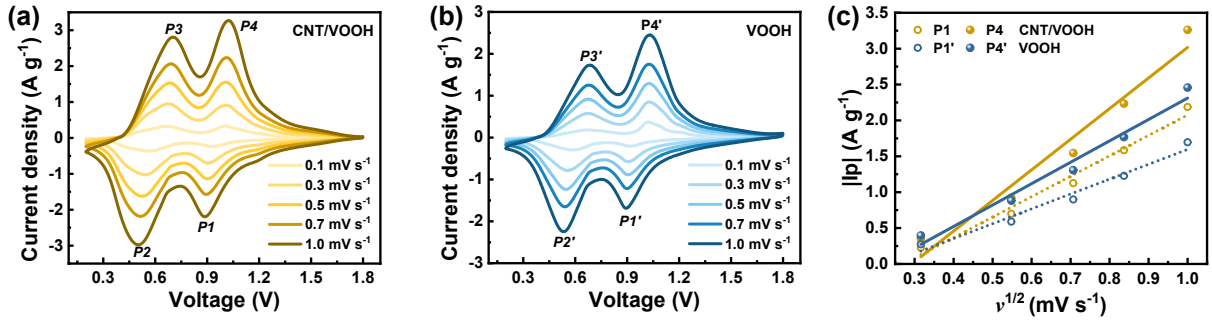

Figure S10. Kinetic analyses. (a-b) CV profiles of the (a) CNT/VOOH and (b) VOOH cathodes under various scan rates from 0.1 to 1.0 mV s^{-1}. (c) The linear fitting of I_p *vs* $v^{1/2}$ for each redox peak of CNT/VOOH and VOOH in a-b.

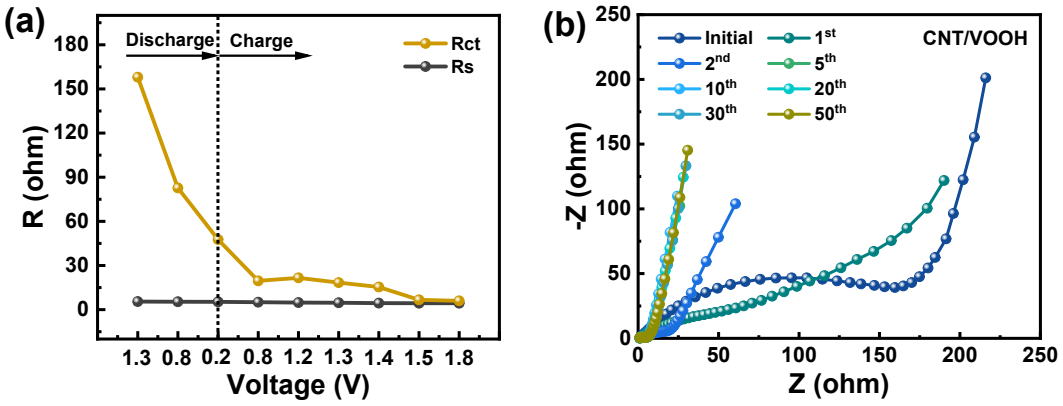

Figure S11. (a) *In-situ* measurement of resistance of CNT/VOOH cathode during first discharge and charge. (b) *In-situ* EIS profiles of CNT/VOOH cathode after selected cycles.

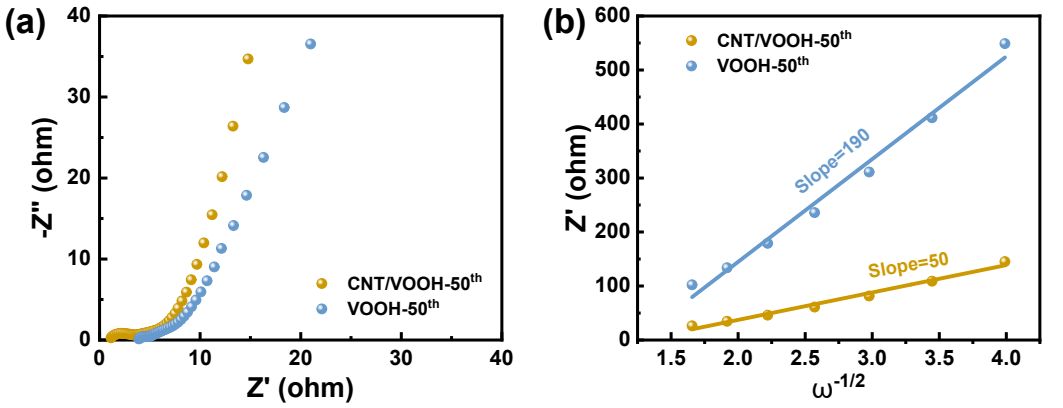

Figure S12. (a) EIS profiles and (b) the linear fitting of Z_{real} *vs* $\omega^{-1/2}$ at low frequencies of CNT/VOOH and VOOH cathodes after 50 cycles.

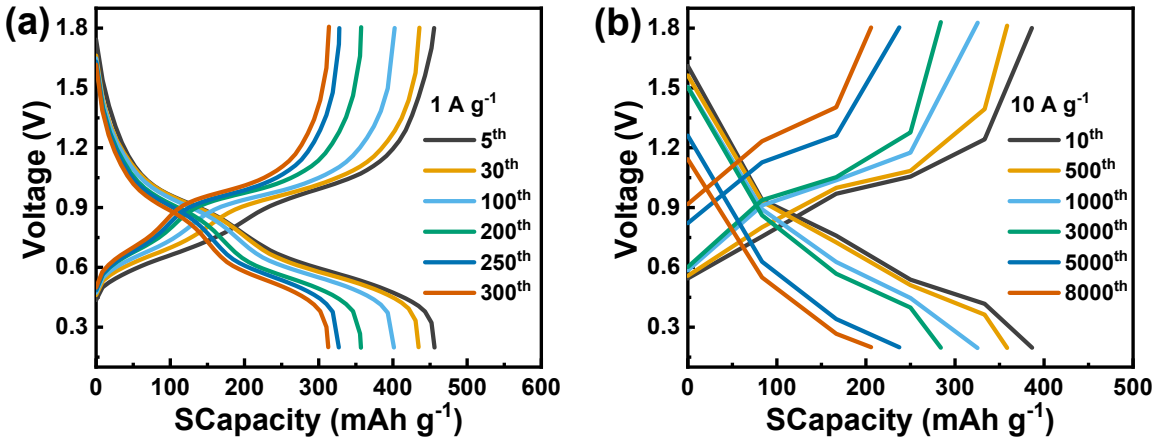

Figure S13. (a) Selected discharge and charge profiles of CNT/VOOH for AZIBs at (a) 1 A g^{-1} and (b) 10 A g^{-1}.

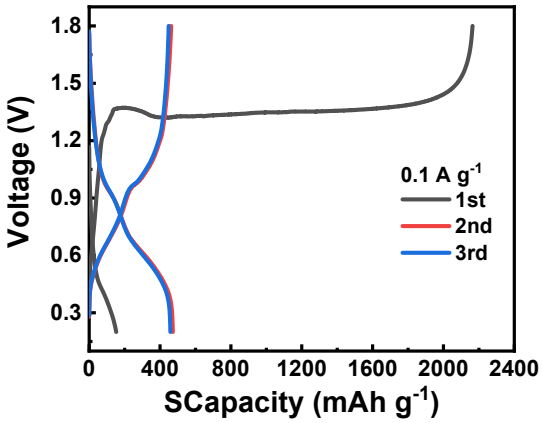

Figure S14. Charge-discharge potential profiles of the AZIBs at 0.1 A g^{-1} by using CNT/VOOH cathodes with an active material percentage of 95 wt.% and Zn metal anode with a thickness of 10 μm (N/P ratio = 2.3).

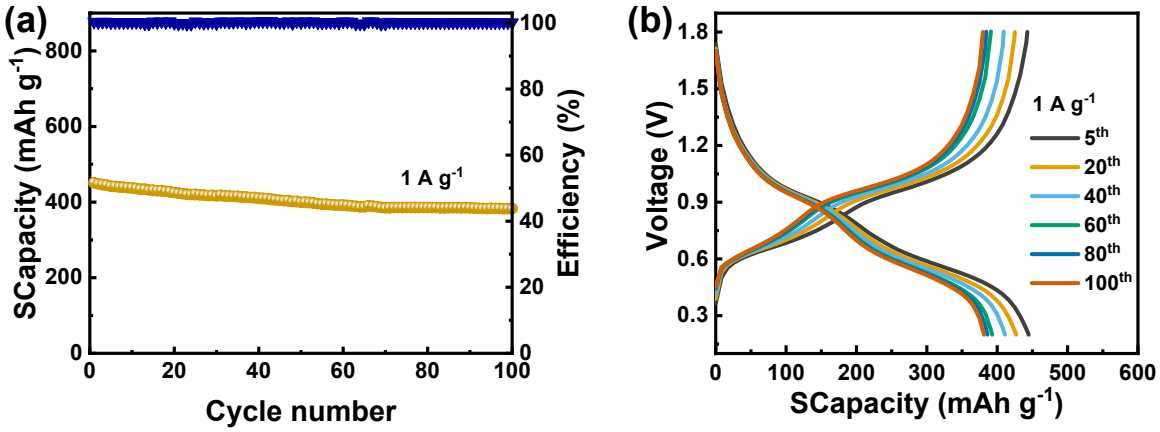

Figure S15. (a) Cycling performance at 1 A g^{-1} and (b) Discharge and charge potential profiles of the CNT/VOOH cathodes with an active material percentage of 95 wt.%.

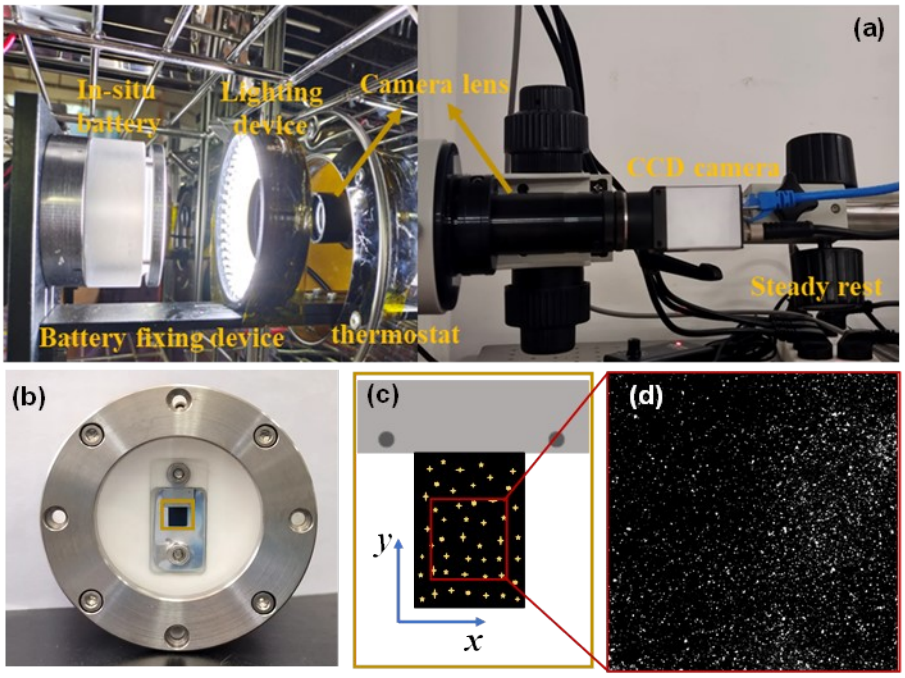

Figure S16. (a) Optical images of the homemade operando strain test system. Schematic diagram of (b) home-made battery, (c) cantilever electrode, and (d) speckle pattern of the region of interest (ROI) on the electrode surface.

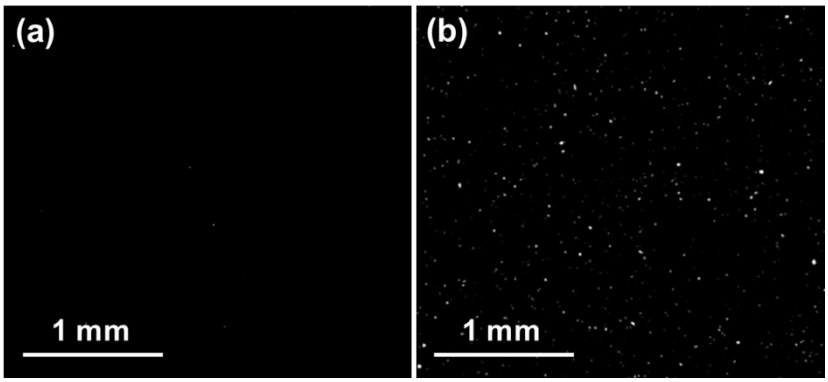

Figure S17. Comparison of the optical images of the cantilever electrode surface (a) before and (b) after addition of graphite particles.

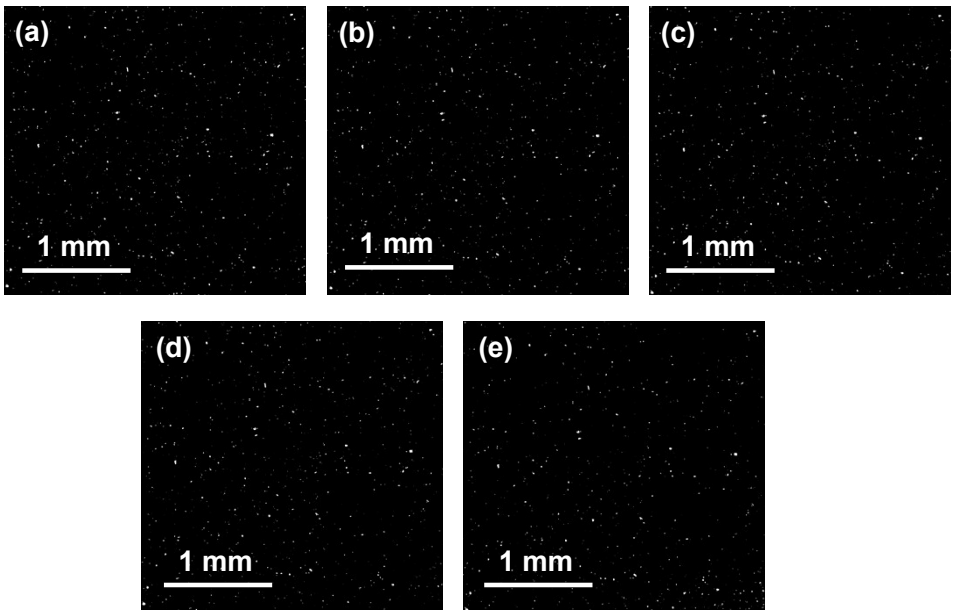

Figure S18. Optical images of the CNT/VOOH cantilever electrode during the cycling process. (a) initial state, (b) discharged to 0.56 V, (c) discharged to 0.20 V, (d) charged to 1.00 V, (e) charged to 1.80 V.

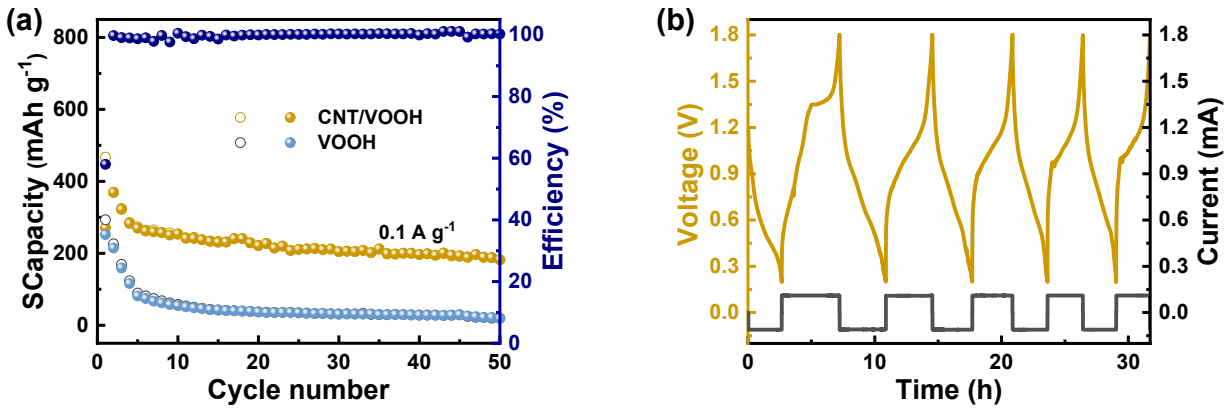

Figure S19. (a) Cycling performance at 0.1 A g^{-1} and (b) Voltage/current-time profiles tested using the homemade cells and the cantilever electrode.

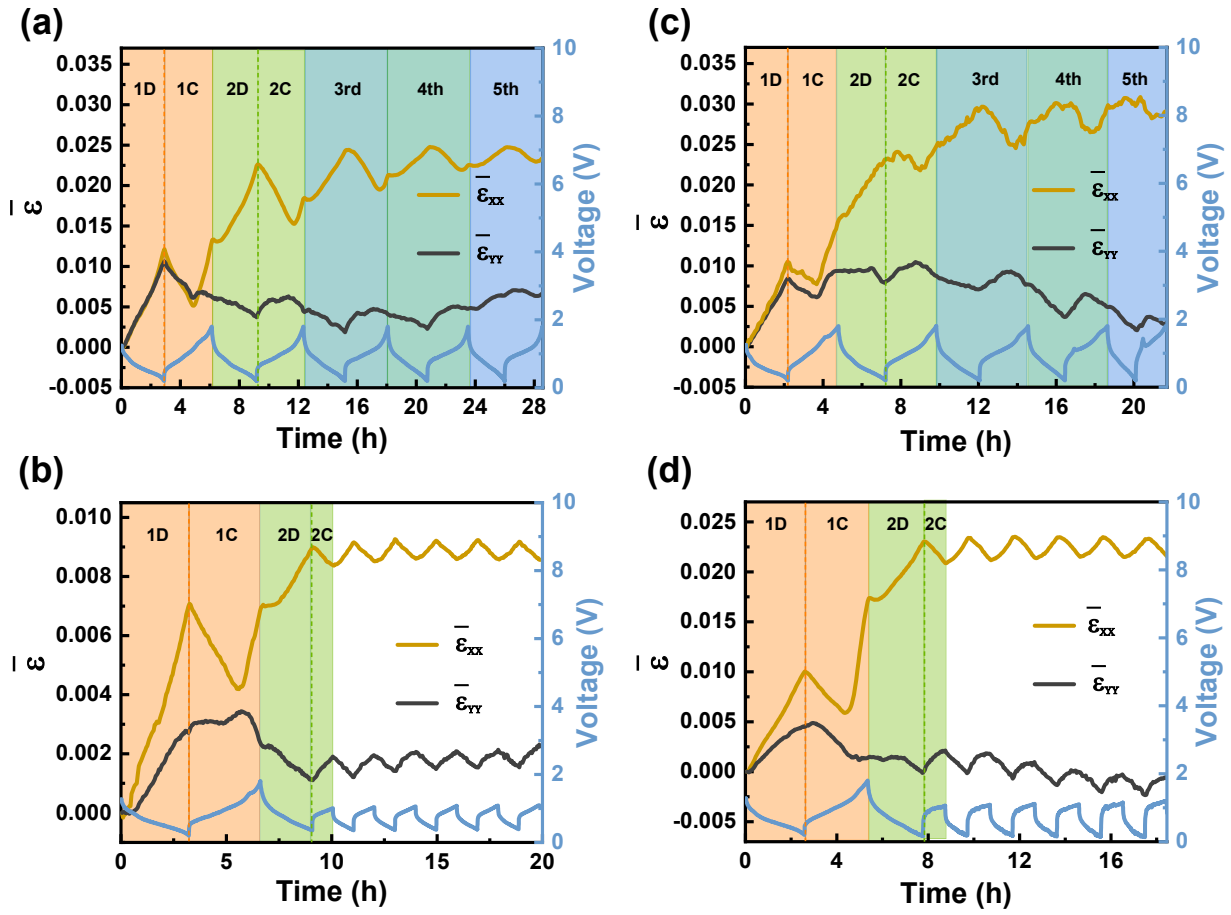

Figure S20. Strain/voltage-time curves of (a, c) CNT/VOOH and (b, d) VOOH under (a, b) limited voltage and (c-d) limited capacity.

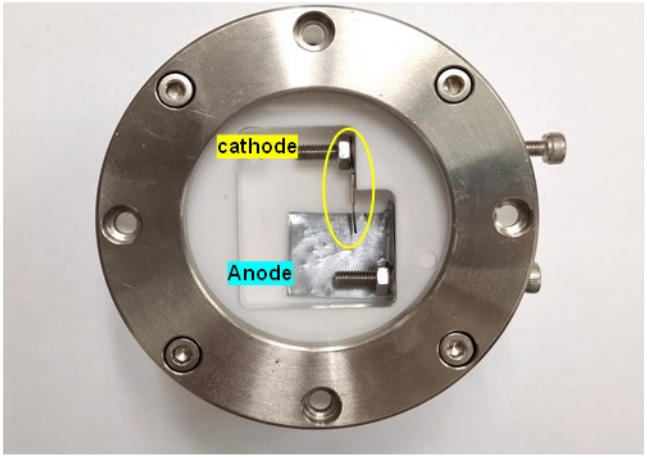

Figure S21. Optical image of a home-made battery with the side of the cantilever electrode parallel to the CCD camera.

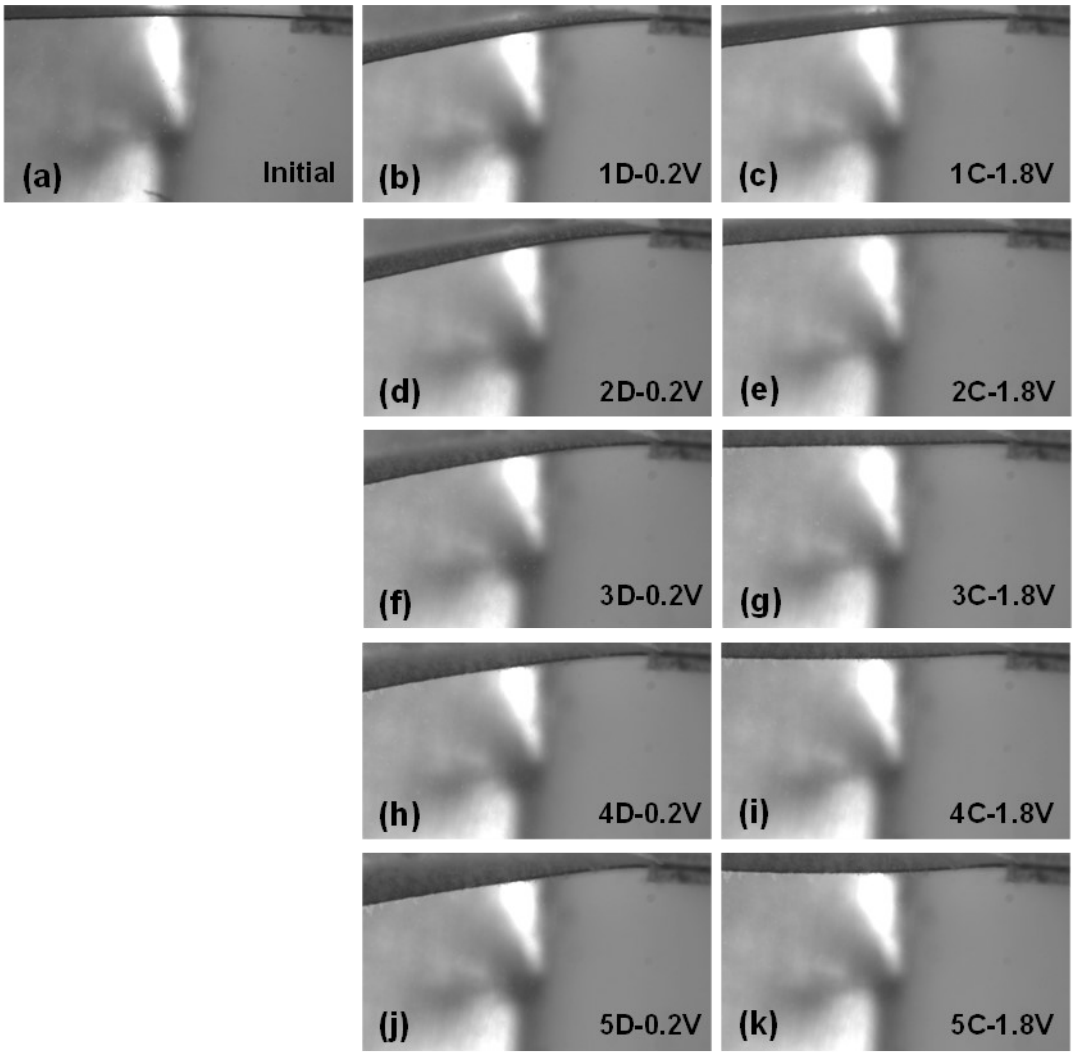

Figure S22. Optical images of the side of the CNT/VOOH cantilever electrode during the cycling process at (a) initial state, (b, d, f, h, j) discharge to 0.2 V, (c, e, g, i, k) charge to 1.8 V.

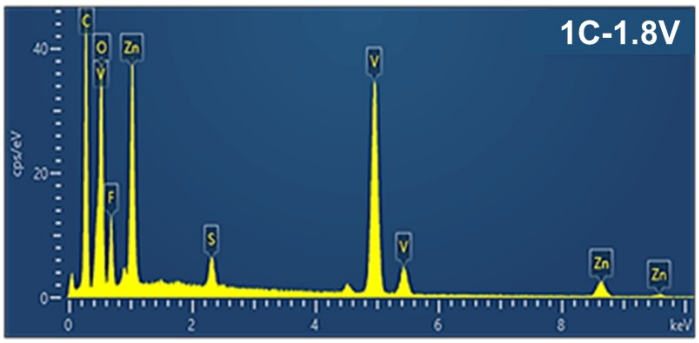

Element	Wt	Atomic
V	40.00%	17.35%
Zn	9.32%	3.15%
Zn/V	0.23	0.18

Figure S23. EDS spectrum and the corresponding element contents of CNT/VOOH when initially charged to 1.8 V.

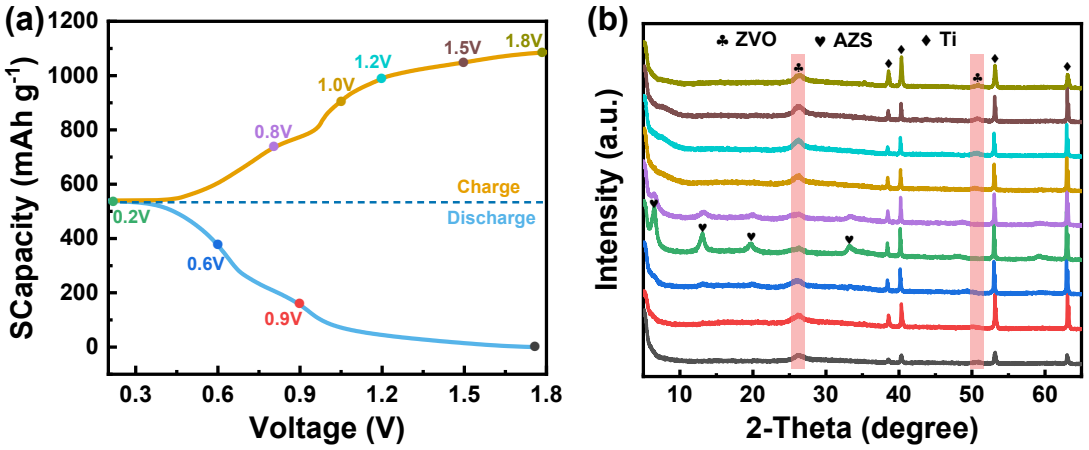

Figure S24. The second discharge/charge voltage profiles (a) and ex-situ XRD patterns of CNT/VOOH at various discharging/charging states (b).

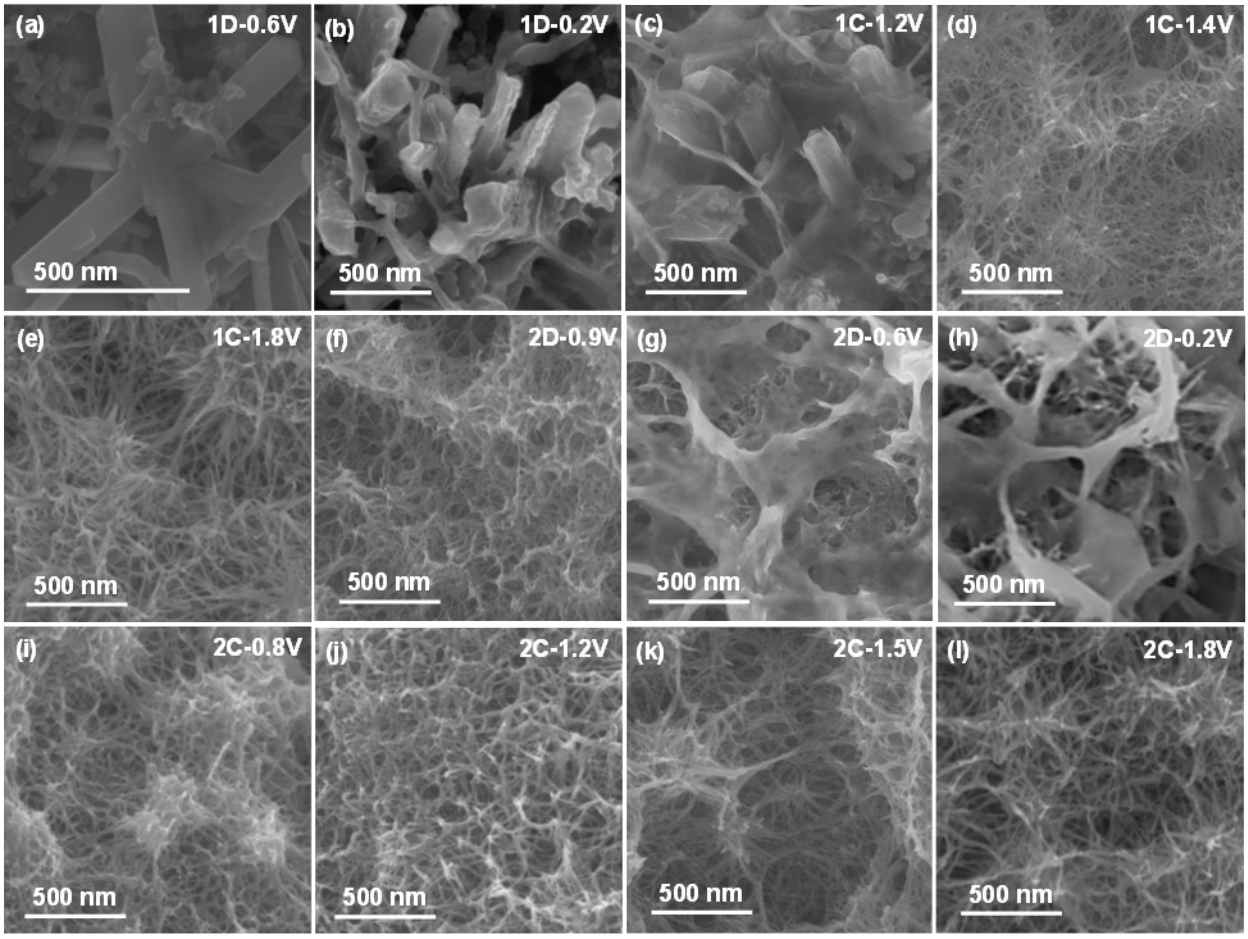

Figure S25. Morphology changes of the CNT/VOOH electrode at different voltages (a) 1D-0.6 V, (b) 1D-0.2 V, (c) 1C-1.2 V, (d) 1C-1.4 V, (e) 1C-1.8 V, (f)2D-0.9 V, (g) 2D-0.6 V, (h) 2D-0.2 V, (i) 2C-0.8 V, (j) 2C-1.2 V, (k) 2C-1.5 V, and (l) 1C-1.8 V. Here, D and C mean the discharge and charge, respectively.

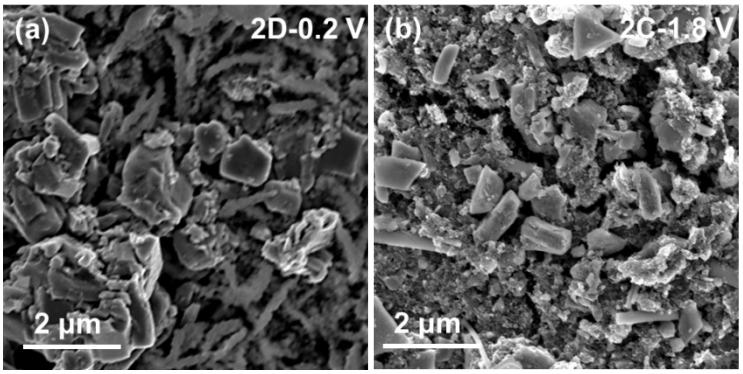

Figure S26. Morphology changes of the VOOH electrode at different voltages (a) 2D-0.2 V, (b) 2C-1.8 V.

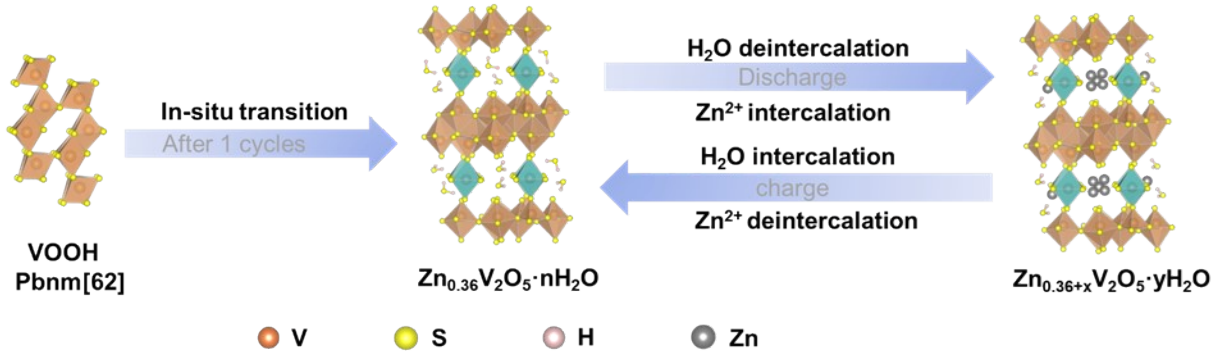

Figure S27. Schematic illustration of the reaction mechanism of CNT/VOOH electrode during cycling.

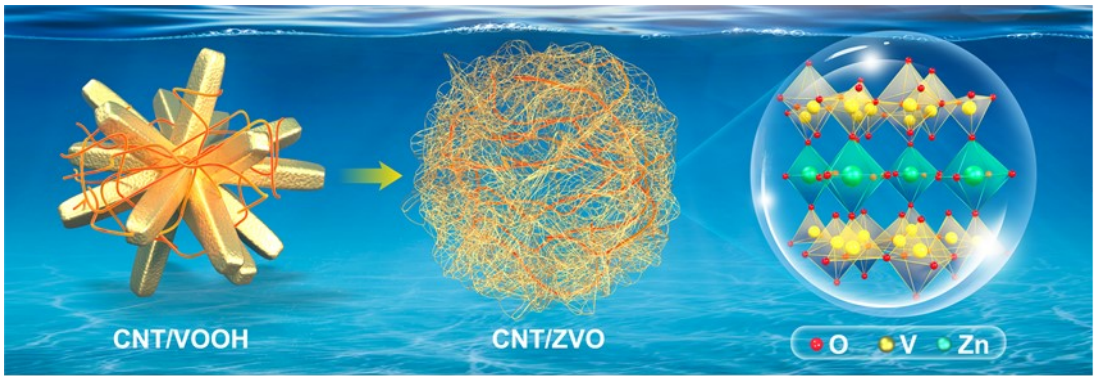

Figure S28. Schematic illustration of the transition from CNT/VOOH to CNT/ZVO.

Table S1: Comparison of the electrochemical performance of the reported vanadium-based materials for AZIB cathodes.

Materials	Current density ($A\ g^{-1}$)	Cycle number	Capacity ($mAh\ g^{-1}$)	**Rate capability ($mAh\ g^{-1}$ /$A\ g^{-1}$)**	Cut-off voltage (V)	Ratio of active materials	Ref.
VO-OH	5	2000	204	**83/20**	0.3-1.5	80%	[4]
$Al_{2.65}V_6O_{13}\cdot 2.07H_2O$	5	2000	182	**376/5**	0.2-1.4	70%	[5]
$Zn_{0.36}V_2O_5 \cdot H_2O$	5	5000	270	**348/5**	0.2-1.8	70%	[6]
VOOH-150	4	2000	150	**80/10**	0.1-1.45	70%	[7]
$Ni_{0.24}V_6O_{13}$	1	100	276	**40/10**	0.2-1.4	70%	[8]
P-Co-NVO	10	3000	161	**124/20**	0.3-1.25	70%	[9]
PANI-V_2O_5	1	900	245	**190/5**	0.2-1.6	70%	[10]
Na-VO_2	12	156	300	**121/10**	0.2-1.6	70%	[11]
VCN NFs	5	1000	45	**73/10**	0.4-1.4	70%	[12]
VOH-rG	10	5000	267	**190/20**	0.2-1.6	70%	[13]
$KV_5O_{13}\cdot 1.3H_2O$.	4	4000	369	**313/10**	0.2-1.6	70%	[14]
Od−HVO@PPy	10	1000	159	**252/10**	0.2-1.6	70%	[15]
$VOPO_4\cdot 2H_2O$	5	2000	158	**168/10**	0.2-1.9	80%	[16]
V_2O_5/MXene	10	5000	110	**243/5**	0.2-1.6	80%	[17]
CNT/VOOH	**1** **10**	**300** **8500**	**319** **206**	**352/10** **322/20**	**0.2-1.8**	**70%**	**our work**

Table S2: Comparison of the N/P ratios for evaluation of the potential of AZIBs for practical applications.

AZIBs	N/P ratio	Ref.
Zn|$NaV_3O_8 \cdot 1.5H_2O$	5	[18]
Zn|$NH_4V_4O_{10}$	8	[19]
SLM-Zn|MnO_2	3.3	[20]
3DGs@Zn|V_2O_5	1.74	[21]
FCOF@Zn-MnO_2	2	[22]
Zn|CNT/VOOH	**2.3**	**our work**

References

[1] X. L. Shi, Q. Q. Yao, H. F. Wu, Y. Zhao and L. H.Guan, *Nanotechnology* **2019**, 30, 465402.

[2] Z. Y.Xu, X. L.Shi, X. Q. Zhuang, Z. H.Wang, S. Sun, K. K.Li and T. Y. Zhang, *Research* **2021**, 2021, 9842391.

[3] E.M.C. Jones, N.R. Sottos, M.N. Silberstein and S.R. White, *Experimental Mechanics* **2014**, 54, 971–985.

[4] Y. Li, S. Zhang, S. Wang, Z. Xiao, F. Meng, Q. Li, X. Zhang, Z. Zhang, L. Zhi, Z. Tang, *Adv. Energy Mater.*, **2023**, 2203810.

[5] T. Lv, G. Zhu, S. Dong, Q. Kong, Y. Peng, S. Jiang, G. Zhang, Z. Yang, S. Yang, X. Dong, H. Pang, Y. Zhang, *Angew Chem. Int. Ed.*, **2023**, *62*, 202216089.

[6] X. Zhang, F. Xue, X. Sun, T. Hou, Z. Xu, Y. Na, Q. An, Z. Chen, S. Cai and C. Zheng, *Chem. Eng. J.* **2022**, *445*, 136714.

[7] R. Nagraj, R. Puttaswamy, P. Yadav, H. K. Beere, S. N. Upadhyay, N. Sanna Kotrappanavar, S. Pakhira and D. Ghosh, *ACS Appl. Mater. Interfaces*, **2022**, *14*, 56886-56899.

[8] Z. Chen, J. Hu, S. Liu, H. Hou, G. Zou, W. Deng and X. Ji, *Chem. Eng. J.* **2021**, *404*, 126536.

[9] M. Du, Z. Miao, H. Li, F. Zhang, Y. Sang, L. Wei, H. Liu and S. Wang, *Nano Energy* **2021**, *89*, 106477.

[10] R. Li, F. Xing, T. Li, H. Zhang, J. Yan, Q. Zheng and X. Li, *Energy Stor. Mater.* **2021**, *38*, 590-598.

[11] Y. Liu and X. Wu, *Nano Energy* **2021**, *86*, 106124.

[12] Y. Y. Liu, G.-Q. Yuan, X. Y. Wang, J.-P. Liu, Q. Y. Zeng, X. T. Guo, H. Wang, C. S. Liu and H. Pang, *Chem. Eng. J.* **2022**, *428*, 132538.

[13] H. Luo, B. Wang, F. Wu, J. Jian, K. Yang, F. Jin, B. Cong, Y. Ning, Y. Zhou, D. Wang, H. Liu and S. Dou, *Nano Energy* **2021**, *81*, 105601.

[14] N. Qiu, Z. Yang, R. Xue, Y. Wang, Y. Zhu and W. Liu, *Nano Lett.* **2021**, *21*, 2738-2744.

[15] Z. Zhang, B. Xi, X. Wang, X. Ma, W. Chen, J. Feng, S. Xiong, *Adv. Funct. Mater.*, **2021**, *31*, 2103070.

[16] Z. Wu, C. Lu, F. Ye, L. Zhang, L. Jiang, Q. Liu, H. Dong, Z. Sun, L. Hu, *Adv. Funct. Mater*., **2021**, *31*, 2106816

[17] H. Liu, L. Jiang, B. Cao, H. Du, H. Lu, Y. Ma, H. Wang, H. Guo, Q. Huang, B. Xu, S. Guo, *ACS Nano*, **2022**, *16*, 14539-14548.

[18] Y. Wang, Z. Wang, W.K. Pang, W. Lie, J.A. Yuwono, G. Liang, S. Liu, A.M.D. Angelo, J. Deng, Y. Fan, K. Davey, B. Li, Z. Guo, Nat. Commun., 2023, 14, 2720.

[19] T. Wei, Y. Ren, Y. Wang, L.'e. Mo, Z. Li, H. Zhang, L. Hu, G. Cao, ACS Nano, 2023, 17, 3765-3775.

[20] S. Wu, S. Zhang, Y. Chu, Z. Hu, J. Luo, Adv. Funct. Mater., 2021, 31, 2107397.

[21] B. Wu, B. Guo, Y. Chen, Y. Mu, H. Qu, M. Lin, J. Bai, T. Zhao, L. Zeng, Energy Stor. Mater., 2023, 54, 75-84.

[22] Z. Zhao, R. Wang, C. Peng, W. Chen, T. Wu, B. Hu, W. Weng, Y. Yao, J. Zeng, Z. Chen, P. Liu, Y. Liu, G. Li, J. Guo, H. Lu, Z. Guo, Nat. Commun., 2021, 12, 6606.